MARS 2001 ODYSSEY

NEUTRON SPECTROMETER PROCESSING

Version 1.3

06/30/2004

Prepared By:
Tom Prettyman,
Dot Delapp,
Bill Feldman,
and Sylvestre Maurice

Table of Contents

1. Introduction 3
2. RoadFit 4
2.1. Objective 4
2.2. Theory 4
2.3. Algorithm 8
3. Validate 10
3.1. Objective 10
3.2. Category 1 Spectrum Processing 10
3.2.1. Correction for differential nonlinearity 11
3.2.2. Using gain data from RoadFIt 12
3.2.3. Gain correction 12
3.2.4. Net Peak Areas 13
3.3. Category 2 spectrum processing 15
3.4. Altitude correction 15
3.5. Other processing issues 16
3.6. The Output of Validate 16
4. Bellyband 16
4.1. Theory 17
4.2. Implementation 17
5. Post Processing with IDL 18
References 20

1. INTRODUCTION

This document describes the processing steps for the reduction of neutron counting data acquired by the neutron spectrometer subsystem on Mars Odyssey. Additional information on the neutron spectrometer can be found in the literature: A general overview of the data reduction process is given by *Prettyman et al.* [2004]. A detailed description of the neutron spectrometer instrument and basic data products is given by *Feldman et al.* [2002] and *Boynton et al.* [2004].

A series of data processing codes have been written to convert Level 0 raw neutron counting data to Level 1 Derived Neutron Data (DND), a time series of corrected neutron counting data that can be used for scientific investigations. The Level 1 data set also includes Averaged Neutron Data (AND), which consists of maps of neutron count rates determined from the DND time series.

An overview of the Level 0 to Level 1 process is shown in Fig. 1. For routine processing, LANL uses the University of Arizona's query tool to download Neutron Spectrometer data for selected time intervals. The queried data set used for the development of data products for PDS delivery is Extended LANL with spatial and extra (BCE #55). This data set includes the raw neutron counting data as well as ancillary Level 1 data, including instrument state of health information and SPICE data, needed to support neutron data reduction and analysis.

The raw data are processed sequentially by three codes, RoadFit, Validate, and Bellyband, to produce the DND time series. RoadFit provides a coarse survey of the raw data, including information about the time-dependent drift of the instrument gain and the flux of energetic charged particles. This information is used to manually edit the data set to exclude periods of time that cannot be analyzed using subsequent codes, including times when the instrument gain shifts rapidly or when there is a solar energetic particle event. Validate uses information from RoadFit to determine count rates from pulse height spectra acquired by the spectrometer during each collection interval (approximately 20s on average, but variable due to flight hardware and software interactions). In addition, Validate filters out a portion of the data set that is unsuitable for science analysis. Rejection criteria are included for periods of time when the energetic particle background is elevated and times when the instrument is not stable or spacecraft operations interfere with the acquisition of mapping data. Finally, Bellyband determines coarse variations in the count rate caused by instrument drift and variations in neutron production by galactic cosmic rays. This information is used in post processing codes to normalize the data output by Validate to produce the DND.

The Level 0 data set includes two categories of counting data: Category 1 refers to single interactions with a boron-loaded plastic, sensitive element (prism); and Category 2 refers to double time-coincident interactions within one or two prisms. Level 1 thermal and epithermal neutron counting data are determined from the Category 1 data. Fast neutron counting data are determined from the Category 2 data.

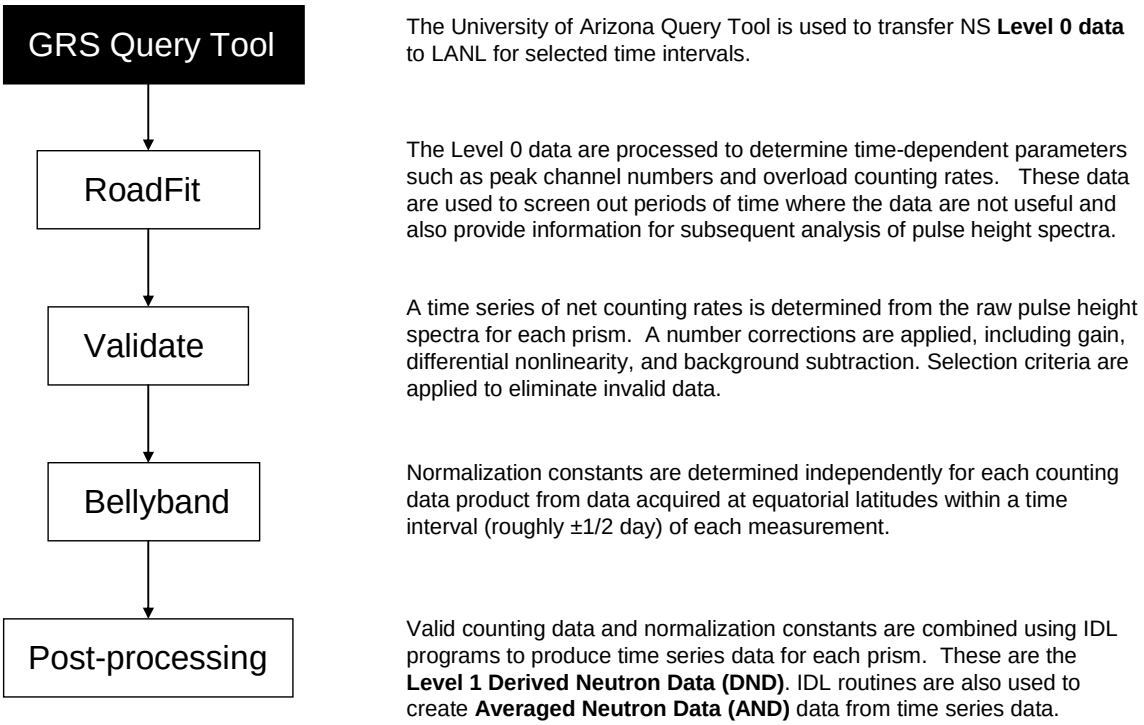

Figure 1. Overview of data processing steps.

2. ROADFIT

2.1. OBJECTIVE

The purpose of RoadFit is to determine the centroid of the $^{10}B(n,\alpha)$ peak and the after-pulse threshold of each prism of the spectrometer over coarse time intervals. This information is used in subsequent codes to determine net peak areas from Category-1 (single interaction) pulse height spectra. The ^{10}B peak centroid is also a useful monitor of the overall gain of each prism, which varies with applied high voltage and phototube performance. The overload counting rate (averaged over 720 collection intervals) is also output by the code to enable manual editing of the data set to filter out significant solar energetic particle events. The overload counter records events that deposit energy in the prisms above a threshold (approximately 2.5 MeV equivalent electron energy) and is useful for monitoring energetic particle events. The overload rate is recorded in the DND time series.

2.2. THEORY

RoadFit uses the Category-2 double pulse events to acquire background-free spectra needed to determine the peak centroid and threshold for each prism. This signature is primarily the result of interactions of fast neutrons with the spectrometer, which originate from cosmic ray

showers that occur in the spacecraft and planetary surface. Fast neutrons are identified by the detection of a characteristic, double pulse. The light output caused by proton recoils produced by the prompt interaction of a fast neutron and the hydrogen in the plastic provides a measure of the energy of the incident neutron. A second pulse of light corresponding to the absorption of the neutron at low energy by ^{10}B follows a delay in which the neutron is slowing down in the plastic, but does not produce light. This double-pulse signature occurs for neutrons above approximately 700 keV. A diagram of a fast neutron interaction is shown in Fig. 2.

Time-correlated double pulses can also occur when high energy particles interact with the plastic scintillators. These pulses can distort the shape of the fast-neutron spectrum if they are not eliminated. They are caused when an energetic particle deposits energy in the plastic, causing a large pulse of light. The associated photomultiplier tube can emit a characteristic "after pulse" caused by the production of secondary electrons through the impact of ions on the photocathode, dynodes, or the residual gas in the tubes. The drift of ions occurs on the time scale of the neutron die-away time. So, time discrimination is ineffective in suppressing these events. However, the second pulse is usually well below the pulse height of the $^{10}B(n,\alpha)$ peak, and setting a lower level threshold is sufficient to eliminate after-pulsing.

A typical second event spectrum is shown in Fig. 3. The spectrum contains a low energy peak associated with after-pulsing, a peak at 93 keVeq associated with the recoil of the reaction products following neutron capture by 10B, and a continuum which is caused by additional energy deposition by the 478 keV gamma ray produced by the decay of $^{7}Li^{*}$ produced by neutron capture on ^{10}B. The relatively low continuum underneath the 93 keVeq peak enables accurate determination of the peak centroid.

The effect of after pulsing is illustrated in Fig. 4 for Category 2 events acquired for Prism 4, which was found to be the most susceptible to after pulsing. For each double pulse event, the amplitude of the first and second pulse is determined along with the time between the pulses. An event mode buffer enables this information to be recorded for 84 events each 19.75s measurement interval. Events can be accumulated over many intervals to determine the distributions of time intervals and pulse heights.

The time to second pulse distribution is shown on the left of Fig. 4 for all events (labeled "uncorrected" in the figure). This spectrum contains fast neutron events as well as after-pulse events and chance coincidences. The peaks that appear at early times correspond to He and Ar atoms present in the phototube and that are ionized during the first pulse and form a second pulse when they impact on the dynodes or photocathode. Setting a lower level threshold on the second event spectrum above the first peak eliminates these time features as can be seen in the corrected spectrum. The lower threshold also has a significant effect on the spectrum of first pulses as shown on the right of Fig. 3. The corrected first pulse spectrum is related to the energy distribution of incident fast neutrons and is therefore useful for science investigations of the planetary surface.

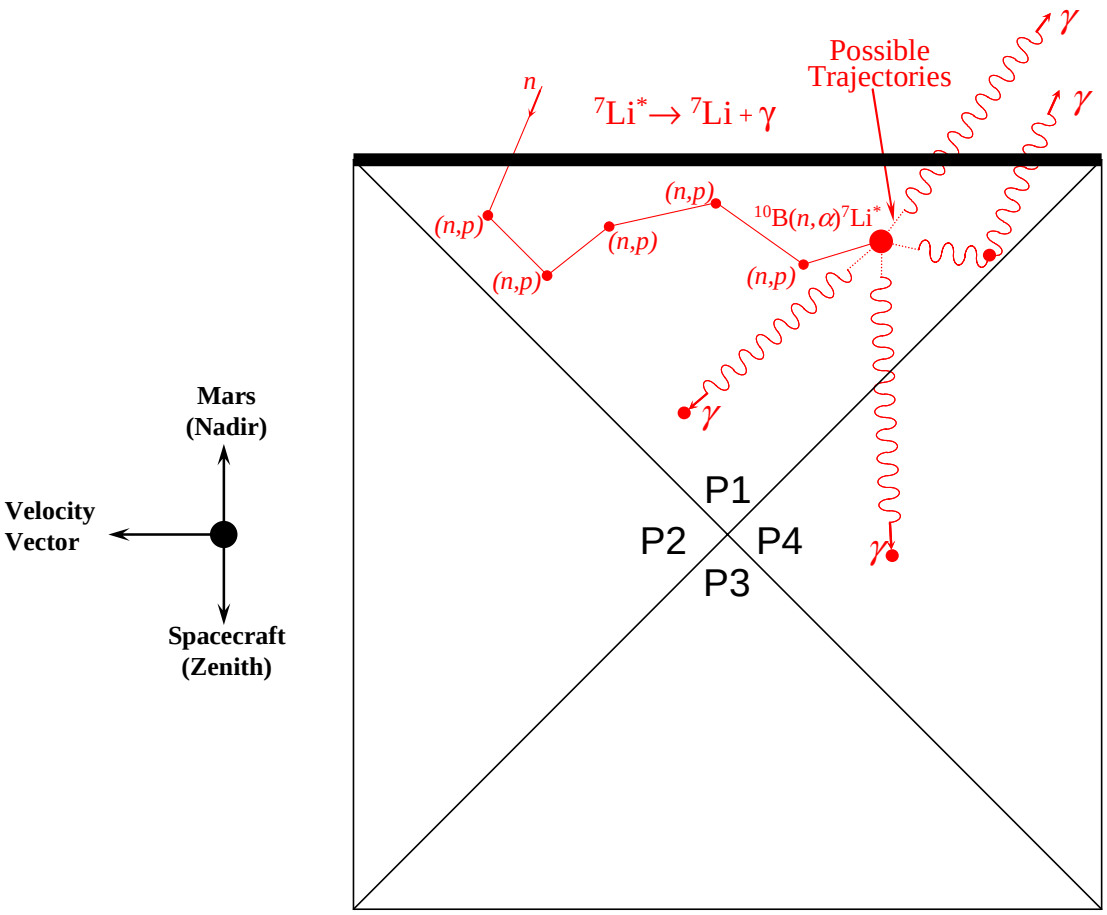

Figure 2. The arrangement of sensitive elements (prisms) is shown along with a diagram of a fast neutron interaction. The neutron spectrometer consists of a block of boron-loaded plastic that is diagonally segmented into four optically decoupled prisms that are viewed by separate photomultiplier tubes. During mapping, two of the prisms are aligned along the axis of motion of the spacecraft: Prism 2 (P2) faces in the forward direction and Prism 4 (P4) faces opposite to the direction of motion. The remaining two prisms are oriented along the nadir axis: Prism 1 (P1) faces downward towards Mars and Prism 3 (P3) faces upwards towards the spacecraft. P1 is covered with cadmium foil, which absorbs neutrons below roughly 0.5 eV. Consequently, P1 is sensitive to epithermal neutrons.

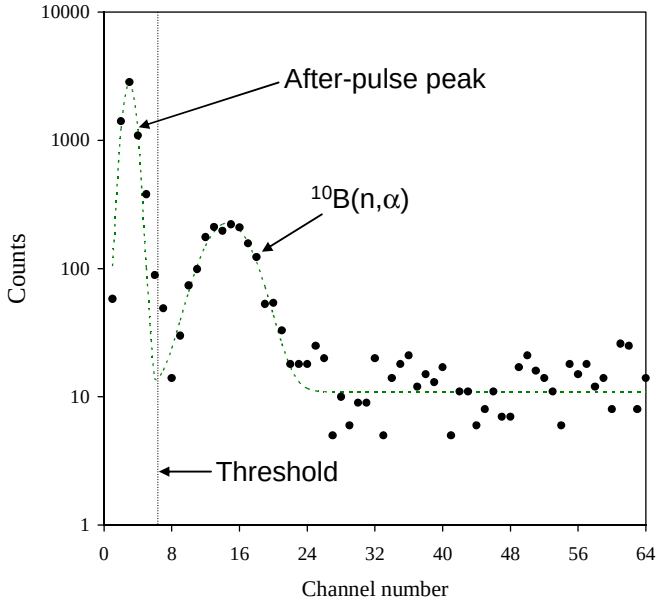

Figure 3. Spectrum of second events summed over 720 collection intervals.

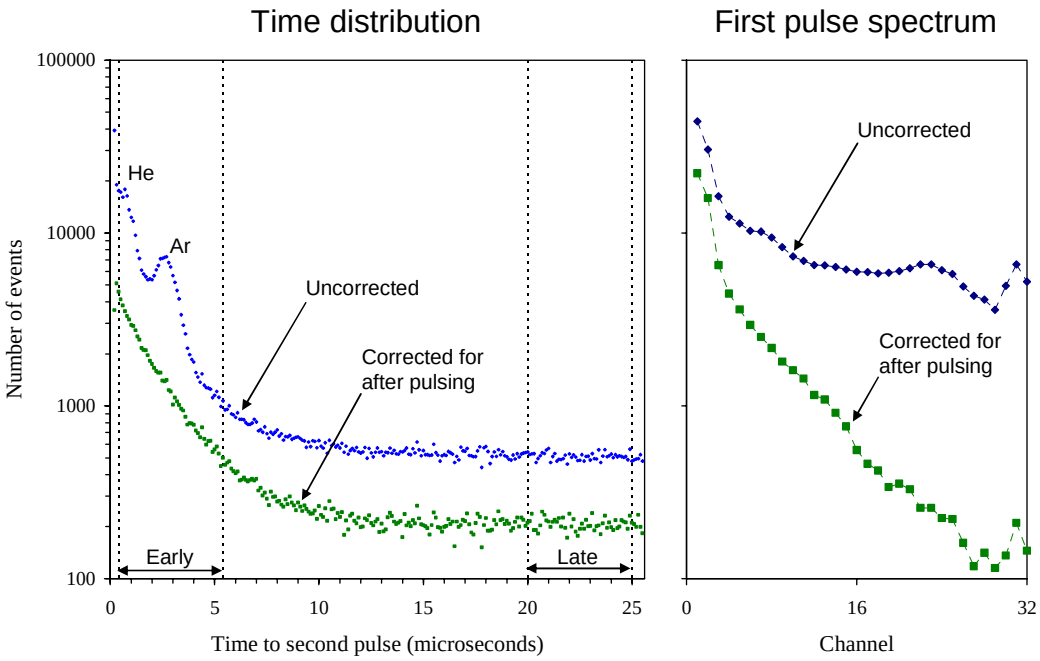

Figure 4. The time distribution of second pulses is shown on the left for an arbitrary time interval during which the gain was stable. The uncorrected distribution was constructed using all events acquired during the time interval. The corrected spectrum was constructed using only those events above the after pulse threshold (channel 7 of the second event pulse-height spectrum in this example. The pulse height spectrum of first interactions is shown on the right before and after correction for after-pulsing.

2.3. ALGORITHM

Category-2 event mode data are accumulated over a coarse time window containing 720 collection intervals. The overload counts are monitored and events are discarded for intervals for which the overload counts exceed a user-defined upper threshold. Anomalously low counts are also excluded using a lower threshold. For each time window, the second event spectrum is constructed from the accumulated event-mode data. If the number of accepted intervals is less than 360, then the time window is not analyzed and the window is assigned the results for centroid and threshold from the analysis of the previous window.

The second event pulse height spectrum acquired for each window was analyzed by simultaneously fitting two Gaussian distributions (one for the ^{10}B peak and one for the after-pulse peak) and a constant background (to represent the continuum) to the data. An example fit is shown in Fig. 3. The fitting algorithm minimizes the sum of the squares of the difference between the model and the data weighted by the statistical uncertainty in the counting data – in other words, a weighted least squares fit to the data. The model is given by

$$M_j = a_0 \exp\left(a_1 j^2 + a_2 j\right) + a_3 \exp\left(a_4 j^2 + a_5 j\right) + a_6, \quad (1)$$

where j is the channel number (between 1 and 64). The fitting routine uses the IMSL (Fortran math library) routine DUNLSF to solve the non-linear least squares problem using a modified Levenberg-Marquardt algorithm with a finite difference Jacobian.

The first two exponential terms are normal distributions describing the peaks in the spectrum. The peak centroids are given by $C_1 = -a_2/(2a_1)$ and $C_2 = -a_5/(2a_4)$, respectively. The full width at half maximum of each peak is given by $FWHM_1 = 2.35\sqrt{-1/(2a_1)}$ and $FWHM_2 = 2.35\sqrt{-1/(2a_4)}$, respectively. The peak with the highest centroid is taken to be the ^{10}B peak. The threshold for after-pulsing is taken to be the channel for which the model is minimum between the centroids of the two peaks.

The centroid of the ^{10}B peak and the threshold channel are output by RoadFit for each time window. In addition, the time (as measured by SCLK seconds since 1-Jan-1980 from the SFDU) is reported for the end of each window along with the number of collection intervals used to form the second event spectrum and other ancillary data, such as the average overload counts.

Results of RoadFit for Prism 1, including the peak centroid and afterpulse threshold are shown in Fig. 5 as a function of areocentric sun longitude. The ^{10}B peak centroids for all four prisms are given in Fig. 6 as a function of SCLK for data acquired from February 2002 through March 2004. The peak centroid determined by RoadFit is used subsequently by Validate to make gain corrections in the Category 1 single event spectrum. The peak centroids can be seen to drift slowly over time, but also undergo occasional abrupt shifts. Both the drift and abrupt shifts have been linked to variations in the high voltage power supplies. The high voltage monitor is also shown in Fig. 6 for comparison on a scale that has been stretched and shifted.

The average overload counts for each 720 record interval is also output by RoadFit. The overload counting rate, plotted in Figs. 5 and 6, shows peaks due to energetic particle events. Time regions corresponding to these peaks are manually edited from the data set prior to further analysis. Periods of time when the gain shifts rapidly are also edited from the data set. The manual selection of excluded intervals is subjective (Fig. 6).

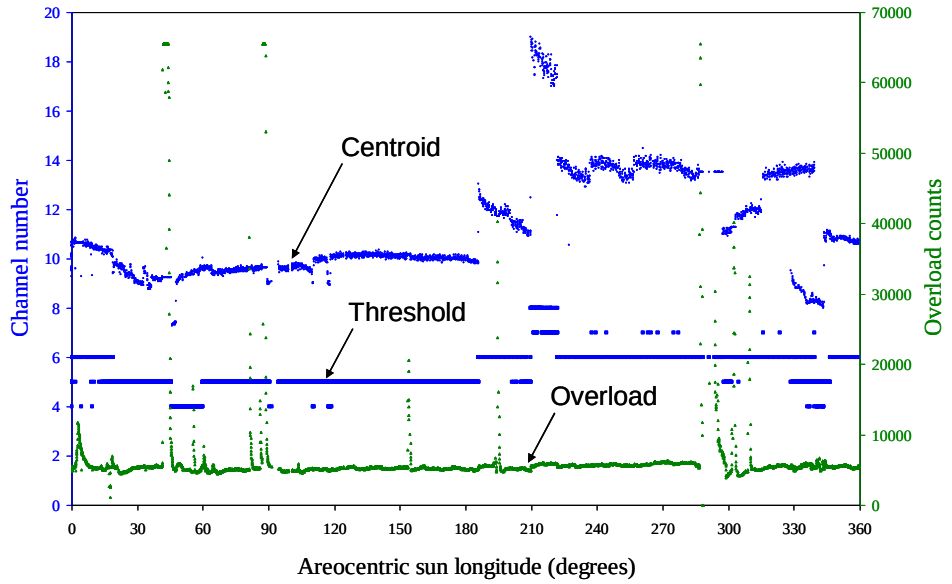

Figure 5. The centroid of the ^{10}B peak and threshold for after pulsing for Prism 1 determined by RoadFit for one Mars year is shown (left axis). The average overload counts is also shown (right axis).

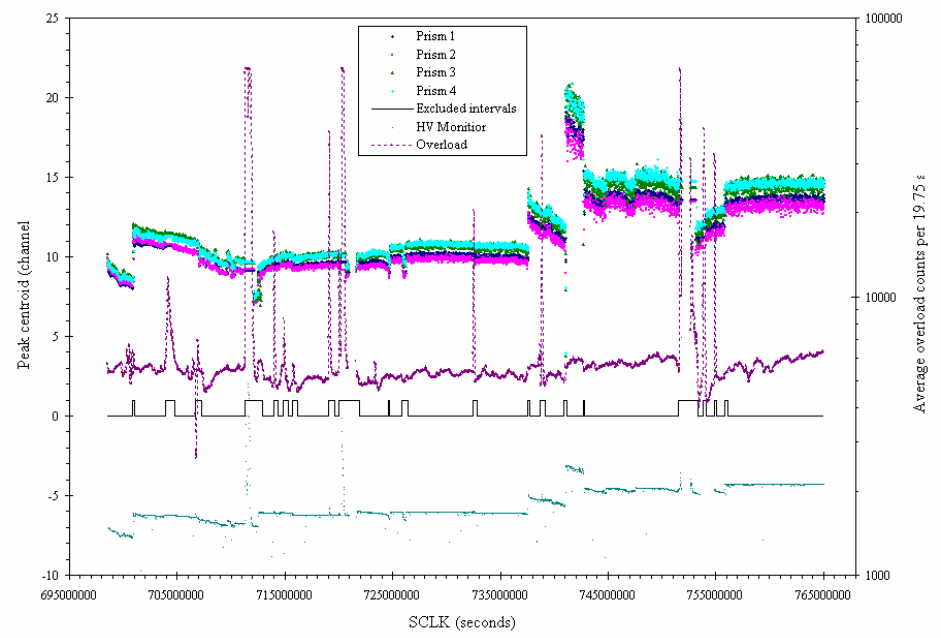

Figure 6. The centroid of the ^{10}B peak is shown for each prism as a function of time (left axis). The average overload counting rate is also shown (right axis). The high voltage monitor value (with units of Volts) was divided by 25 and offset by -40 to produce the trace shown (use the left scale for interpretation). Data excluded from subsequent analysis correspond to times when the excluded interval trace is 1 (using the left scale).

3. VALIDATE

3.1. OBJECTIVE

The purpose of Validate is to determine $^{10}B(n,\alpha)$ counting rates from Category 1 spectra for each prism and Category 2 histogram sums. Validate also provides fine time scale filtering of the data set by excluding individual collection intervals with overload counts that fall outside of a user defined window. Data for which the spacecraft is not pointing in the nadir direction are also filtered from the data set. The end result of Validate is a time series of count rates from which thermal, epithermal, and fast counting data are determined.

3.2. CATEGORY 1 SPECTRUM PROCESSING

The Category 1 data for each prism consists of a 64 channel pulse height spectrum which contains a peak at 93 keV equivalent light output (denoted keVeq) corresponding to the capture of a neutron with energy less than about 700 keV by ^{10}B (Fig. 6). Underneath the peak is a background continuum caused by the interaction of gamma rays originating from Mars and the spacecraft as well as by Compton scattering and escape of the 478 keV gamma ray produced by the decay of $^{7}Li^{*}$, which is produced by neutron capture on boron. The objective of the Category 1 spectrum processing is to extract the net peak area from the spectrum.

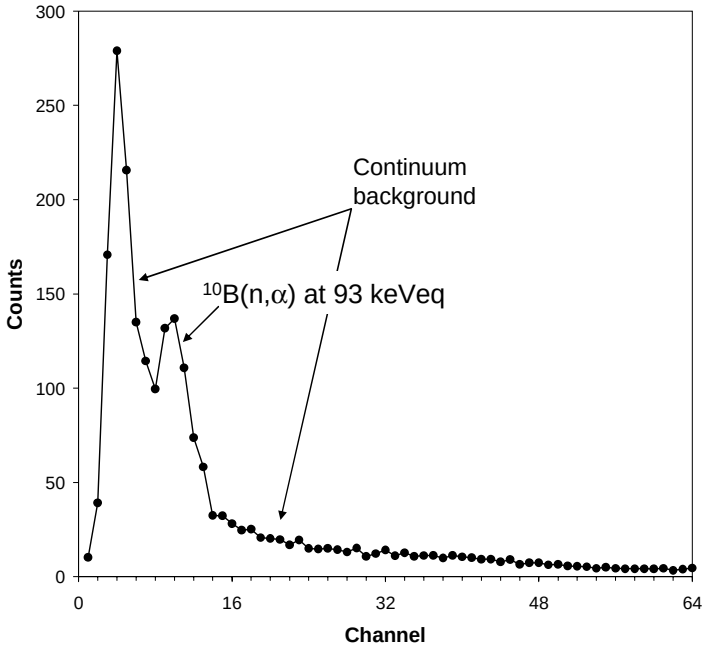

Figure 6. Example Category 1 pulse height spectrum averaged over 51 19.75s counting intervals. No corrections have been applied.

3.2.1. Correction for differential nonlinearity

A correction was applied to each spectrum to remove artifacts of the differential nonlinearity of the analog to digital converter from the spectrum. The differential nonlinearity was determined by averaging spectra from Prism 3 poleward of 85°N over a long time period that includes northern summer (roughly 226 days during mapping). Because Prism 3 is relatively well shielded from neutrons that originate from the planet and the flux of neutrons is low at the pole, the averaged spectrum does not have a $^{10}B(n,\alpha)$ peak and contains only the continuum background, which is expected to vary smoothly in the absence of digitization errors. By smoothing the spectrum (using a 5-channel boxcar filter) and comparing to the unsmoothed data, a repetitive, 16-channel pattern was observed. Based on these data, correction factors were derived for each of the 16 channels. The correction can be applied to the four groups of channels in the spectrum. An example of the application of the differential nonlinearity correction is shown in Fig. 7.

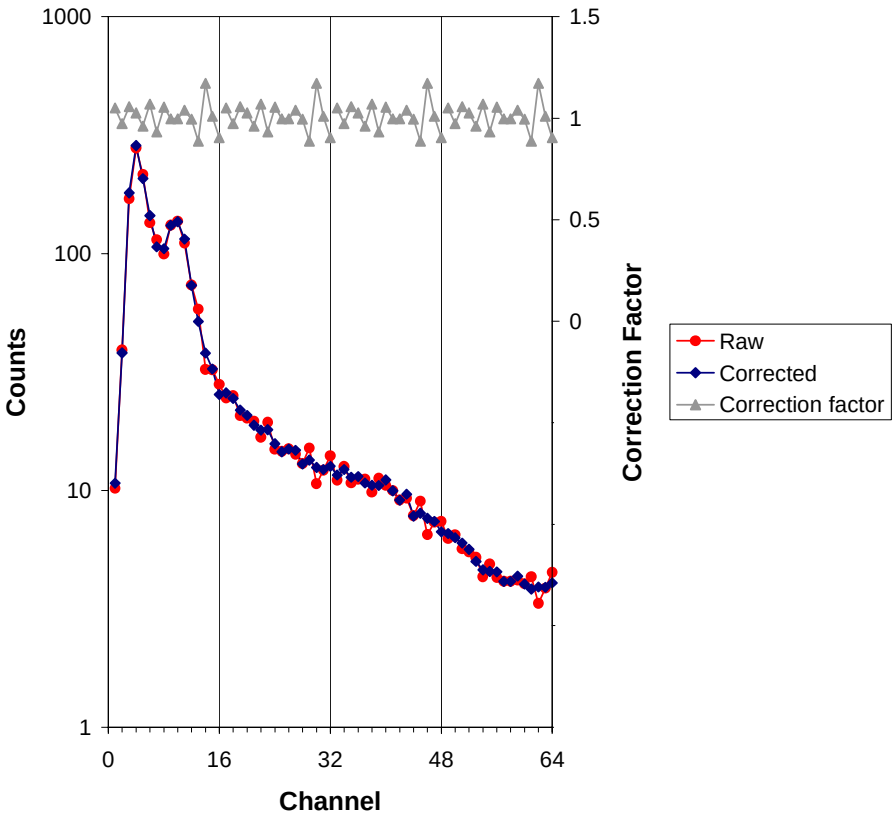

Figure 7. Correction of a Category 1 pulse height spectrum averaged over 51 collection intervals (the raw spectrum is also shown in Fig. 6 on a linear-linear scale). The 16-channel correction factors are applied to each of the four groups of the spectrum. Application of the correction factor reduces the variance in the counting data.

3.2.2. Using gain data from RoadFIt

The peak channels determined by RoadFit from the Category 2 second event pulse height spectra are offset from the peak channels observed in the Category 1 pulse height spectra for two reasons. First, the pulse processing system uses separate gated integrators to process the prompt and delayed pulses from a fast neutron interaction. The gated integrator used to process the second event has a different gain than the gated integrator used for the Category 1 events. The roles of the gated integrators can also be reversed via an uploadable command. On 28-May-2003 (roughly SCLK= 707061818s), the roles of the gated integrators were reversed, which resulted in a reduction in the gain of the second event. So, the relationship between the Category 1 and second event pulse heights changed following this date. Second, the location of the second event is not recorded. While it is most likely that the second event occurs in the same prism as the first interaction, some portion of second events occur in other prisms. Consequently, a systematic bias is introduced into the gain estimate for each prism. Based on the analysis of Category 1 data over a wide range of gain settings, we found that a simple offset was sufficient to convert the second event channel numbers to channel numbers useful for establishing regions of interest about the 93 keVeq peak in the Category 1 data. The offsets are different before and after 28-May-2003 and are given as follows:

- Before 28-May-03 subtract 0.5 to the channel number given by RoadFit for a all prisms
- After 28-May-03:
    - Prisms 1, 3, and 4, add 0.5.
    - Prism 2, add -1.5.

3.2.3. Gain correction

Following the correction for differential nonlinearity, each of the Category 1 prism spectra were corrected for gain so that the 93 keVeq peak fell consistently in a selected channel (Channel 11 in the PDS data set). Implementation of this step requires knowledge of the original peak centroid as determined by RoadFit. The gain correction enables the same region of interest (range of channels) to be used for the peak and background for all spectra.

The gain correction algorithm is implemented in the subroutine gaincor of the Validate program. The algorithm calculates the energy range spanned by each channel in the uncorrected spectrum. The relationship between channel number and energy is assumed to be linear. The slope and offset of are determined using the channel number given by RoadFit for the 93 keVeq peak centroid and an assumed offset (-3 channels). The offset was estimated from low gain spectra acquired over long periods of time for which both the 93 keVeq peak and the Compton edge produced by the 478 keV gamma

ray were visible. The energy range spanned by a channel in the uncorrected spectrum can be mapped onto a range of channels in the corrected spectrum, for which the 93 keVeq peak channel number and offset were selected to be 11 and -3, respectively. The counts in the uncorrected channel are distributed uniformly over the range of channels determined for the uncorrected spectrum. This step is repeated for every channel in the uncorrected spectrum. Counts are conserved in this process except for the uppermost and lowermost channels for which the uncorrected energy scale may fall outside the limits of the corrected spectrum. The results of the correction algorithm are shown in Fig. 8 for a high gain case. A similar approach was used for gain correction of gamma ray spectra from the Lunar Prospector mission [*Lawrence et al*., 2004]

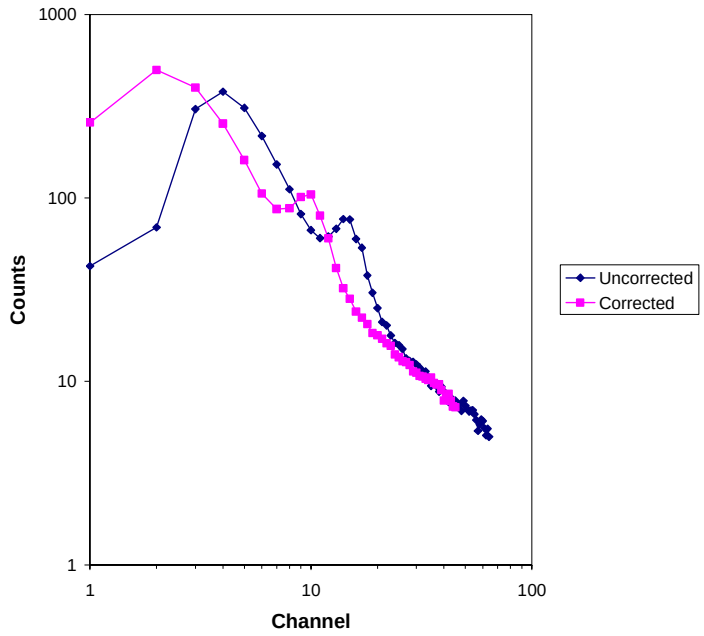

Figure 8. Application of the gain correction algorithm to a Category 1 pulse height spectrum averaged over 51 collection intervals.

3.2.4. Net Peak Areas

Once the gain correction is made, the same set of channels can be used to define the peak region of interest for all measurements. Based on trial and error using data acquired with different gains, the following regions of interest (ROIs) were defined:

Lower background:	Channels 6 and 7
Peak region of interest:	Channels 8 through 15
Upper background region:	Channels 16 through 21

The upper and lower background ROIs are used to determine the background continuum, which was found to be well-represented by a power law with channel

number. The net peak area was determined by subtracting the counts predicted by the power law from the total counts in the peak ROI.

For the present PDS submission, the power law background is determined for the average of spectra within a sliding time window spanning 5 consecutive collection intervals. The length of the window was selected empirically to minimize the uncertainty in the background parameters because of statistical variations in count rate while avoiding the introduction of bias resulting from integration over surface features. The net area is determined by subtracting the average background from the total counts in the peak ROI for the spectrum in the middle of the sliding window. The process is illustrated in Fig. 9.

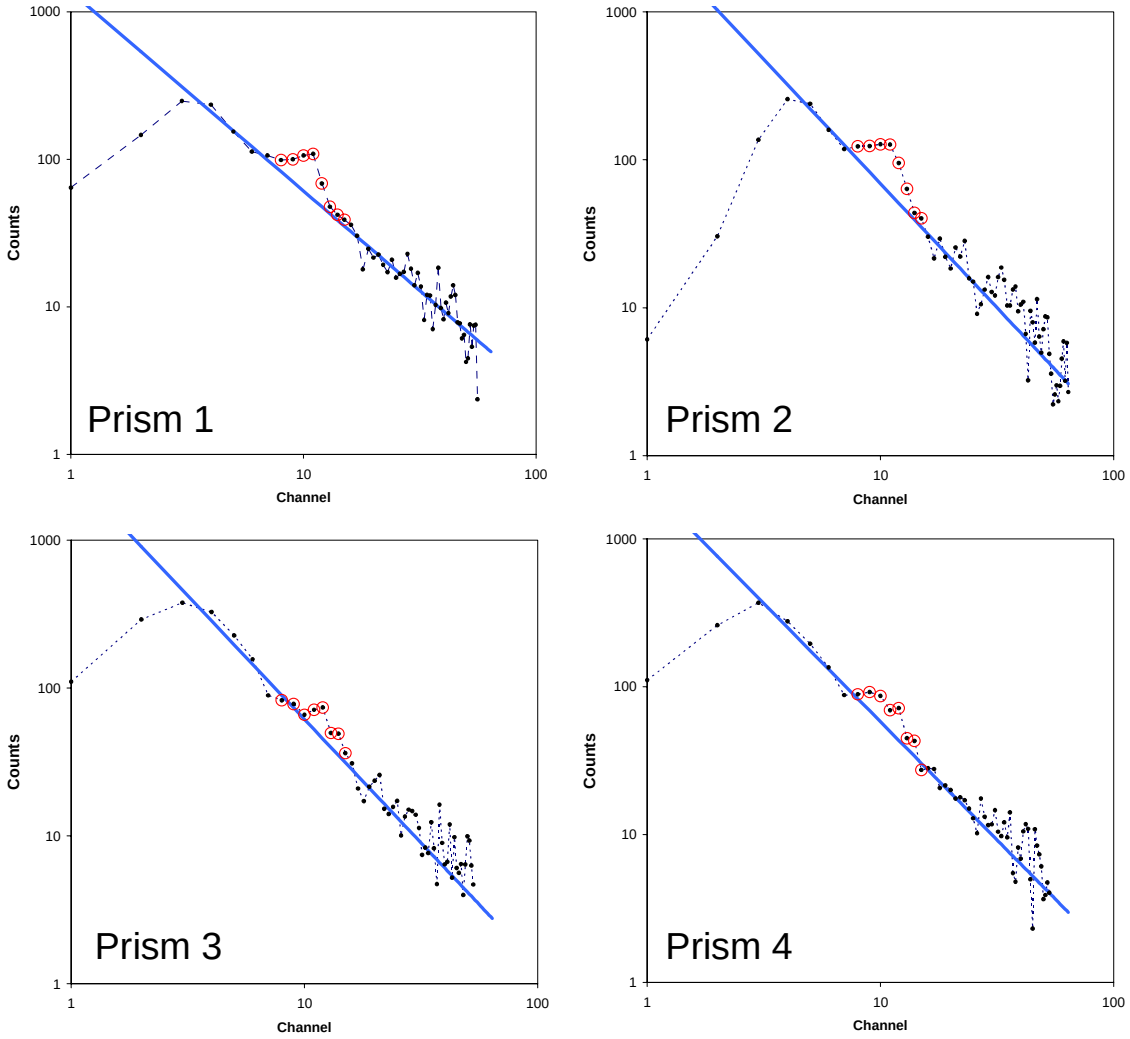

Figure 9. Determination of net peak area for a single collection interval using power law backgrounds determined from the average of 5 collection intervals. The red circles indicate the peak ROI. The blue lines show the power law background.

3.3. CATEGORY 2 SPECTRUM PROCESSING

For fast neutrons (Category 2), two data products are provided in the raw data set: Event-mode data for which the magnitude of the first pulse, time to the second pulse, and magnitude of the second pulse of a selected number of events (84 per collection interval) were recorded; and histogram data for which first pulses with magnitude above a preset, fixed threshold were binned into histograms for early and late time windows. Note that the histogram data are binned on board the spacecraft by the neutron spectrometer's field programmable gate array. All events above a level discriminator are included in the histogram data set. Consequently, the histogram data are used to determine the fast neutron counting rates. The event mode data are provided as a diagnostic (for example, to determine the gain of each prism) and were limited to 84 events per acquisition interval due to limitations in the telemetry rate. The late time interval (nominally chosen to be between 20 and 25 μs) was selected so that it is well beyond the die-away time of neutrons in the spectrometer and thus contains accidental events only. The early time interval (nominally chosen to be between 0.4 and 5.4 μs) was selected so that it is sensitive to neutrons slowing down in the spectrometer. Subtraction of the late from early time histograms yields a pulse-height spectrum that is sensitive to the energy spectrum of fast neutrons. The event-mode data are useful for counting system diagnostics. The histogram data have better counting precision and are therefore preferred for the development of fast-neutron maps and are included in the DND time series.

The fast-neutron count rate was taken to be the first two channels of the histogram spectrum for P1, which is primarily sensitive to neutrons coming directly from Mars. The lower channels were selected because they give the greatest count rates and are also least susceptible to contamination by after-pulsing. However, because considerable drift in gain occurred, the threshold selected for after-pulse suppression used to construct the histogram data was not always effective. During times of high gain, the threshold was too low and after-pulsing events contaminated the histogram spectrum. Variations caused by shifts in gain were corrected using the BellyBand algorithm described in section 4.

3.4. ALTITUDE CORRECTION

The count rate measured by the spectrometer varies with the solid angle subtended by Mars at the spacecraft, which depends on altitude and is given by

$$\Omega(h) = 2\pi\left[1 - \sqrt{1 - R^2/(R+h)^2}\right], \qquad (1)$$

where R is the volumetric mean radius of Mars and h is the altitude of the spacecraft. All count rates are normalized to an altitude of 400 km by multiplying by a correction factor for altitude given by $\Omega(400\text{ km})/\Omega(h)$. The altitude h for each measurement interval is included along with the raw counting data.

3.5. OTHER PROCESSING ISSUES

In order to consider data for inclusion in the time series, we required that the instrument be aligned along the bore-site vector of spacecraft motion and nadir orientation. This eliminated times such as when the spacecraft was in safe mode for which P1 was not pointed in the nadir direction. We also required that the data in the 5 collection interval background buffer be contiguous, separated by no more than 20s in time (as given by the UTC time of at the center of the acquisition interval). This avoided the introduction of errors in the counting data when orbital data were missing. The direction of motion of the spacecraft motion (north or south) was determined from the sign of the difference in latitude between the previous and next collection intervals. The direction information is used to project points forward along the orbital trajectory of the spacecraft (see Section 5). The difference method for determining direction gives reliable results except for the most poleward (north or south) point. The projection algorithm gives approximately the same result for the most poleward points independent of the direction determined by the difference method. Finally, we did not process data for collection intervals for which the overload monitor of the neutron spectrometer was greater than 7000 counts, which corresponded to solar-energetic particle events, or less than 4000 counts.

3.6. THE OUTPUT OF VALIDATE

Validate outputs the following quantities for each measurement interval that meets the analysis acceptance criteria:

- SCLK time (used a unique identifier of the measurement)
- Areocentric longitude (L_S)
- Duration of the collection interval
- Subsatellite latitude and longitude at the center of the acquisition interval
- Net counts for the 93 keVeq peak in the Category 1 spectrum for all four prisms
- The net counts (early minus late) for the first two channels of the Category 2 histogram spectrum for Prism 1

These data are used along with correction parameters developed by BellyBand to determine thermal, epithermal, and fast count rates reported in the DND time series.

4. BELLYBAND

Neutron count rates are sensitive to a number of factors unrelated to the surface and atmosphere of Mars. These include, for example, instrument drift and variations in the galactic

cosmic-ray flux. To eliminate these variations from our data set, we developed an algorithm to adjust our time-series counting data so that count rates at equatorial latitudes did not change with time and were equal to the average count rates observed over a normalization interval, which was arbitrarily selected to be from L_S = 329° to L_S = 131° during the first Mars year of mapping. The region between latitudes ±30° (the "belly band") was used for normalization. Minor variations in count rate due to seasonal changes in atmospheric mass were initially ignored, but were later restored to the time series.

4.1. THEORY

For each 19.75 s measurement interval, belly-band count rates were determined for a time window extending ±6 orbits (a time span of about one Martian day) relative to the location where the measurement was taken, which gives full coverage in longitude of the belly band when the footprint of the spectrometer is considered. To make the correction, the average of the belly-band count rates $\langle C \rangle$ within the time window was found along with the average of the lowest 10% of the belly-band-count-rate population $\langle C \rangle_{10}$. These parameters were used to develop a linear correction whose parameters (slope a and offset b) satisfied the following relationships: $\langle C \rangle_{REF} = a\langle C \rangle + b$ and $\langle C \rangle_{10REF} = a\langle C \rangle_{10} + b$, where $\langle C \rangle_{REF}$ and $\langle C \rangle_{10REF}$ are the average of count rates and the average of the lowest 10% of the count rates, respectively, within the belly band for the normalization interval (L_S = 329° to L_S = 131° during the first Mars year of mapping). The corrected count rate for the selected 19.75-s measurement interval was given by $aC + b$, where C was the count rate before applying the belly-band correction. The correction was applied independently to the fast and Category-1 counting data for each prism.

The belly-band normalization algorithm removes gain and offset variations caused by a number of effects, including variations in the galactic cosmic-ray background and errors in the Category-1 background subtraction algorithm. However, the normalization algorithm also removes variations that would otherwise be present as a result of seasonal changes in atmospheric mass at the equator. Atmospheric corrections are restored during post-processing.

4.2. IMPLEMENTATION

For each 19.75s measurement interval recorded by Validate, Bellyband determines the value of $\langle C \rangle$ and $\langle C \rangle_{10}$ independently for the Category 1 prism counts and the fast neutron counts. Because there are some time gaps in the data recorded by Validate, the number of belly-band records within ±6 orbits is sometimes unacceptably small. If the number of points available is less than a threshold value (1000), then a point is not assigned bellyband data and is excluded from the DND time series during post processing. Bellyband does not apply a correction to the time series data. This is carried out in post processing

5. POST PROCESSING WITH IDL

The objective of the post processing codes is to convert the counting data output by Validate and Bellyband into corrected count rates and to produce the DND and AND data files. This is accomplished by a set of IDL codes, which combine data output from the neutron data reduction codes with Level 1 SPICE and instrument state of health data to produce the final DND data set. The post-processing codes also include a final cut on anomalous collection intervals identified by the analyst.

The post-processing codes read in the Bellyband data files and construct $\langle C \rangle_{REF}$ and $\langle C \rangle_{10REF}$ by averaging data over the normalization interval (L_S between 329 and 131 during the first Mars year of mapping). The belly band correction parameters *a* (slope) and *b* (offset) are calculated using the approach described in Section 4.1. The correction is applied to the uncorrected count rates recorded by Validate. In this process, the counts are divided by the measurement interval live time so that the resulting time series has units of counts per second. The correction parameters and counting data before and after correction are shown in Fig. 10 for Category 1 Prism 2 count rates.

Note that the nominal integration time for each collection interval is 19.75s; however, minor fluctuations about this value occur. The duration for each measurement is recorded and included with the neutron spectrometer raw data for use in normalizing count rates. The dead time, which is the amount of time that the pulse processing electronics is busy processing events and is therefore unavailable to process new events, is also included in the data set. The dead time is recorded by a counter, which can be converted into time in seconds by multiplying by 5.12×10^{-5}. The live time for a measurement is determined by subtracting the dead time from the measurement duration. The average live time during periods of time for which the overload counter was less than 7000 events and greater than 4000 counts per collection interval was 19.42 s. All counting data products are divided by the live time in post processing to determine dead-time-corrected count rates. The count rates are also multiplied by a dimensionless constant, 19.42/19.75=0.9833 to account for the fact that older versions of the processing code did not make dead time corrections and assumed that the live time was 19.75s. This enables published calibration constants for radiation output-response models to be used directly with the PDS data set [*Feldman et al.*, 2003; *Prettyman et al.*, 2004].

Once the belly-band correction has been applied, atmospheric variations are re-introduced to the data set using data from the ARC-GCM. To restore the effect of atmospheric mass, we combined maps of atmospheric mass at equatorial latitudes (derived from the ARC-GCM) with expressions for count rate as a function of atmospheric thickness [*Prettyman et al.*, 2003] to determine the relative variation of belly-band-averaged neutron-counting rates as a function of time. The normalized count rates were then multiplied by the relative variation to restore the atmospheric effect. Use of pressures from the ARC-GCM is justified because the ARC-GCM fits the Viking 1 and 2 landing-site pressure data that are representative of equatorial to midlatitude pressure variations and were found to be reproducible year after year. This procedure was applied to the fast and epithermal counting data in post processing. Thermal neutrons vary negligibly with atmospheric mass when the water abundance of the surface is less

than about 15%, which is representative of the belly band. The fast neutrons, which have the largest variation, show a 5% peak-to-peak variation in count rate over an entire Martian year. Therefore, the correction is relatively minor.

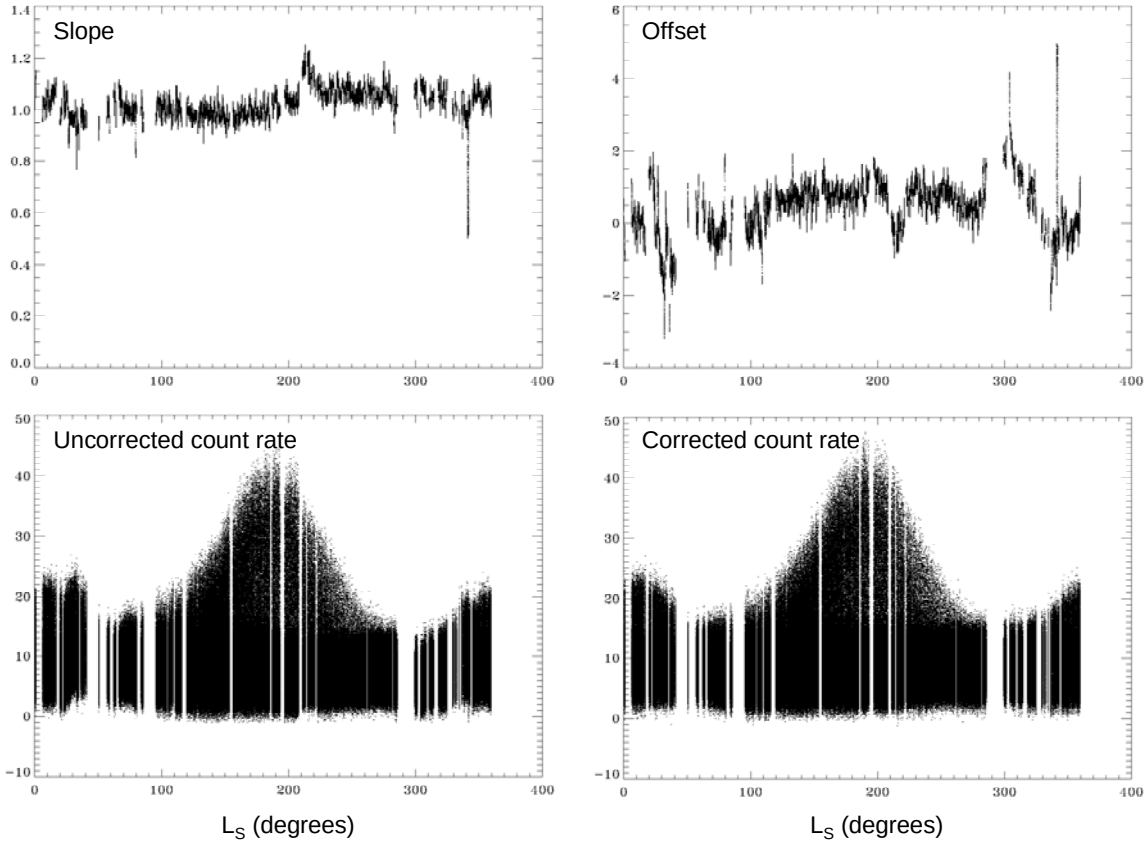

Figure 10. Correction parameters (slope and offset) along with counting data before and after correction are shown for Category 1 Prism 1 count rate data.

The approach for developing thermal, epithermal, and fast count rates from the Category 1 and 2 prism counting data is described elsewhere [*Prettyman et al.*, 2004]. Thermal neutron count rates are calculated as the difference between Category 1, Prism 2 and Prism 4. The fast neutron count rate (Category 2, Prism 1) are adjusted for background using the procedure described by *Prettyman et al.* [2004].

For epithermal and thermal neutrons, there is an aberration in the ram direction (due to the relative motion of the spacecraft and the neutrons) so that the neutrons contributing to the observed count rate tend to originate from ahead of the spacecraft. To correct this aberration, measurements are placed on the map ahead of the sub satellite point, but along the trajectory. To enable this correction, the DND data set includes (longitude, latitude) coordinates for a point shifted 1 degree forward along the orbit from the subsatellite point; and 2) the coordinates for a point shifted 4.5 degrees forward along the orbit. The former is used for mapping epithermal neutrons and the latter is used for mapping thermal neutrons. The magnitude of the shift was

determined based on simulations of the response of P1, P2, and P4 to neutrons at orbital altitudes.

The AND data set consists of maps of thermal, epithermal, and fast neutron count rates averaged over 15º L_S intervals. The maps are determined directly from the DND time series using IDL routines from the Mars Toolkit [*Maurice et al.*, 2002]. The maps are 5º cylindrical projections. In addition to the count rates, maps of the number of measurements binned in each pixel and the standard deviation of the pixel count rates are provided.

REFERENCES

Boynton, W.V., W.C. Feldman, I.G. Mitrofanov, L.G. Evans, R.C. Reedy, S.W. Squyres, R. Starr, J.I. Trombka, C. d'Uston, J.R. Arnold, P.A.J. Englert, A.E. Metzger, H. Wänke, J. Brückner, D.M. Drake, C. Shinohara, C. Fellows, D.K. Hamara, K. Harshman, K. Kerry, C. Turner, M. Ward, H. Barthe, K.R. Fuller, S.A. Storms, G.W. Thornton, J.L. Longmire, M.L. Litvak, A.K. Ton'chev, The Mars Odyssey Gamma-Ray Spectrometer Instrument Suite, *Space Science Reviews*, Volume 110, Issue 1-2, 2004, pp. 37-83.

Feldman, W. C., T. H. Prettyman, R. L., Tokar, W. V. Boynton, R. C. Byrd, K. R. Fuller, O. Gasnault, J. L. Longmire, R. H. Olsher, S. A. Storms, and G. W. Thornton, Fast neutron flux spectrum aboard Mars Odyssey during cruise, *Journal of Geophysical Research - Space Physics*, Vol. 107(#A6) pp. 1083-1083, 2002.

Feldman, W. C., et al. (2003a), CO2 frost cap thickness on Mars during northern winter and spring, J. Geophys. Res., 108(E9), 5103, doi:10.1029/2003JE002101.

Lawrence, D. J., S. Maurice, W. C. Feldman, Gamma-ray Measurements from Lunar Prospector: Time-series Data Reduction from the Gamma-ray Spectrometer, J. Geophys. Res., 10.1029/2003JE002206, 2004, in press.

Maurice, S., D. J. Lawrence, O. Gasnault, IDL Mapping/Display/Support Data Toolkit for the Mars Odyssey GRS and NS Instruments, Los Alamos National Laboratory document LA-CC-0206, 2002.

Prettyman, T. H., W. C. Feldman, M. T. Mellon, G. W. McKinney, W. W. Boynton, S. Karunatillake, D. J. Lawrence, S. Maurice, A. E. Metzger, J. R. Murphy, S. W. Squyres, R. D. Starr, R. L. Tokar, Composition and structure of the Martian surface at high southern latitudes from neutron spectroscopy, J. Geophys. Res., 109, E05001, doi:10.1029/2003JE002139, 2004.